Nanocontact-induced catalytic activation in palladium nanoparticles†

Changlong Jiang,[a] Sadananda Ranjit,[a] Zhongyu Duan,[a] Yu Lin Zhong,[a] Kian Ping Loh,[a] Chun Zhang*[ab] and Xiaogang Liu*[a]

Received 30th May 2009, Accepted 31st August 2009
First published as an Advance Article on the web 29th September 2009
DOI: 10.1039/b9nr00093c

We report the synthesis and catalytic studies of novel palladium nanostructures assembled from small nanoparticles by a surfactant-templated method. These one-dimensional nanomaterials comprise high-density nanocontacts of ~1 nm in contact length at the particle–particle interface. In contrast to dispersed Pd nanoparticles (~5 nm), the polycrystalline palladium nanowires exhibit enhanced (~200 times) catalytic reactivity towards carbon–carbon cross-couplings under mild conditions. Theoretical modeling studies suggest that the presence of nanocontacts triggers electron transfer and localized charge redistribution in the contact region. The charge redistribution causes the nanocontacts to become highly attractive to charged organic molecules, resulting in the facilitation of organic transformations.

An important goal in catalyst research is to establish model systems that enable the desirable activity and selectivity to be achieved *via* an economical process.[1–3] Transition metal-based homogenous catalysts show remarkable activity and selectivity during organic transformations, but suffer from a lack of recyclability and high cost of waste disposal. In contrast, metal nanoparticle catalysts are advantageous over their homogeneous counterparts in terms of easy separation from reaction mixtures and high level of recoverability, but are generally less selective and active. In this regard, there has been considerable recent interest in the rational design and shape-controlled synthesis of metal or metal-oxide nanostructures that offer both superior catalytic efficiency and recyclability.[4–11] We reason that the introduction of nanocontacts[12–15] between nanoparticles should significantly impact material reactivity for organic synthesis, as metallic nanocontacts are known to exhibit different characteristics in electronic, optoelectronic, electrical and magnetic properties from individual non-interacting nanoparticles. Here, we report the synthesis of novel palladium (Pd) nanostructures composed of a network of nanoparticles with high-density point contacts between the particles. We present theoretical modeling and experimental evidence for significant nanocontact-induced catalytic activation of the nanomaterials for cross-coupling reactions in water-based solvents and at ambient conditions.

The formation of Pd nanomaterials with high-density nanocontacts was achieved by a low-temperature solution reaction using poly(*N*-vinylpyrrolidone) (PVP) as a stabilizing ligand. PVP has been well studied as a polymeric capping reagent for the shape-controlled formation of metal nanoparticles and nanowires.[16–19] In our studies, we employed trace copper powder as a reducing agent to control the slow rate of particle growth and subsequently the formation of high density nanocontacts at the particle–particle interface. A plausible mechanism for the nanocontact formation is shown in Scheme 1. Pd ions were first reduced by the copper metal to form Pd nanoparticles, which were subsequently assembled into one-dimensional nanostructures *via* the PVP template. Upon annealing at 50 °C without stirring for 24 h, Pd nanowires comprising a network of nanocontacts were synthesized in nearly quantitative yield. It should be noted that the PVP concentration employed in the synthesis dictates the shape of the as-prepared nanomaterials. For example, only dispersed small particles (~5 nm in average diameter) were formed in the presence of 0.0025 mmol PVP (Fig. S1 of the ESI†). As the concentration of PVP increases, the rate of particle aggregation becomes predominant, resulting in the formation of uniformly interconnected particle nanowires (Fig. S1).

The surface morphology and crystal structure of the as-synthesized nanowires were characterized by SEM, XRD, TEM, and XPS. The results are summarized in Fig. 1. As evident from SEM, these nanowires have a uniform morphology with an average diameter of 100 nm (Fig. 1a). High-magnification SEM shows that each individual nanowire consists of corn-like elongated particle assemblies (Fig. 1b). The XRD pattern of the Pd nanowires is shown in Fig. 1c. All peaks can be indexed to

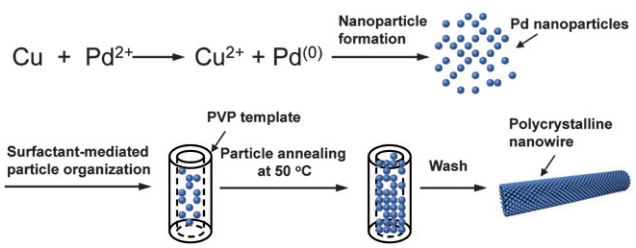

Scheme 1 A schematic illustration of formation of Pd nanocontacts and nanowire growth.

[a]*Department of Chemistrys, National University of Singapore, Singapore 117543. E-mail: chmlx@nus.edu.sg; Fax: +65-65161791*
[b]*Department of Physics and Centre for Computational Science and Engineering, National University of Singapore, Singapore 117543. E-mail: phyzc@nus.edu.sg*

† Electronic supplementary information (ESI) available: Detailed information on the materials and methods used to fabricate and characterize the Pd nanocontacts and nanowires. See DOI: 10.1039/b9nr00093c

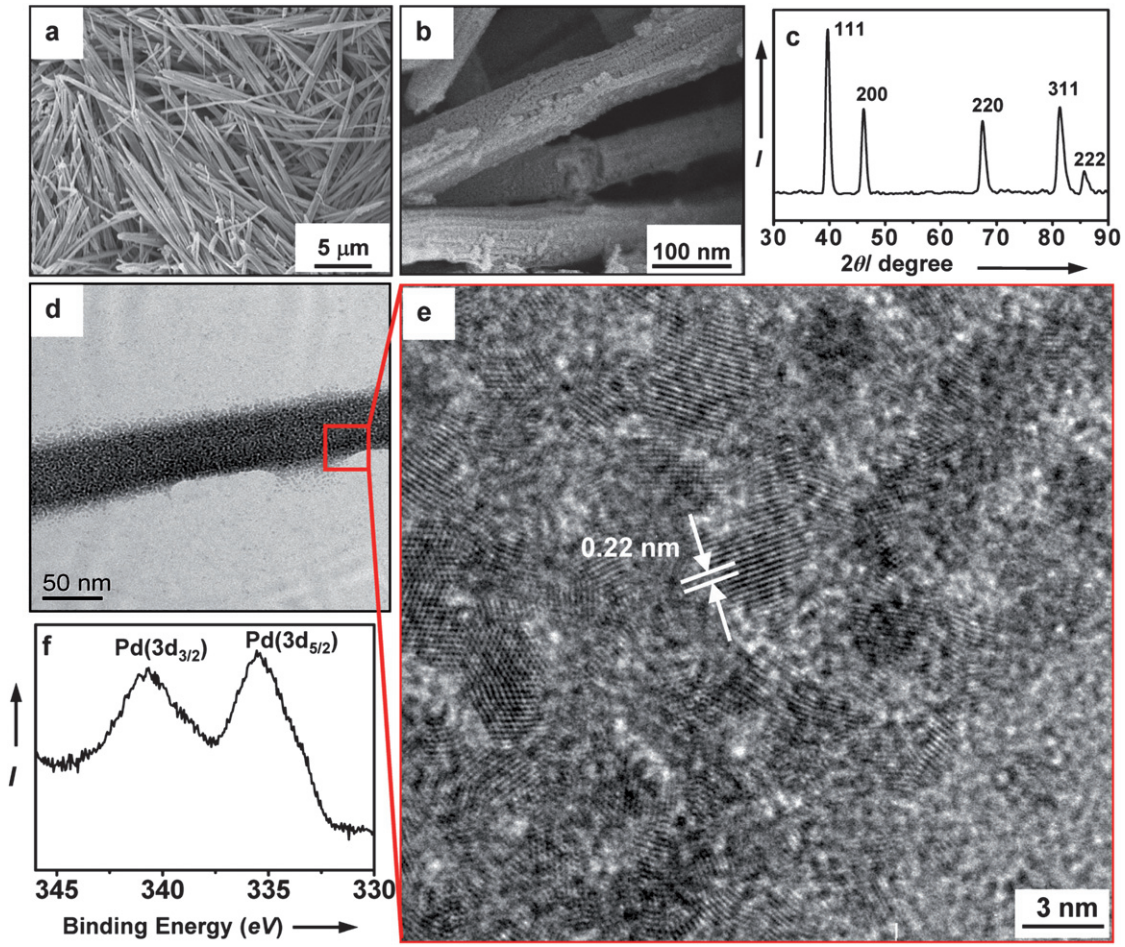

Fig. 1 (a) SEM image of the as-synthesized Pd nanowires. (b) High-magnification SEM image showing surface morphology of the nanowires. (c) X-ray powder diffraction pattern of the nanowires. (d) TEM image of a single Pd nanowire. (e) High-magnification TEM image of the nanowire shown in Fig. 1d. (f) XPS spectrum of the nanowires.

face-centered cubic Pd (Joint Committee on Powder Diffraction Standards Card No. 05-0681). We attribute the peak sharpening to the particle aggregation resulting from the formation of high-density nanocontacts. In agreement with SEM studies, TEM shows densified nanoparticle arrays along the long axis direction of the nanowire (Fig. 1d). A three-dimensional web of interconnected particles (~5 nm in diameter) can be visually traced from the outer edge of the nanowire by high-resolution TEM (Fig. 1e). Lattice fringe analysis shows high-density nanocontacts between the nanoparticles, indicating the polycrystalline nature of the nanowire. The fringe distance of 0.22 nm corresponds to the {111} planes of the Pd (Fig. 1e). The porous network structure has a pore size distribution centered at 5 nm and a surface area of 45 $m^2\ g^{-1}$. (Fig. S3 of the ESI†). The elemental composition of the as-prepared nanowires was determined by XPS. The Pd ($3d_{5/2}$) and Pd ($3d_{3/2}$) peaks were observed at 335.48 and 340.67 eV respectively, which are the characteristic values for Pd metal (Fig. 1f).

In a further set of experiments, the nanowires were examined for catalytic activity during Suzuki cross-coupling reactions under very mild conditions. Several phenyl halides were first examined for their ability to react with phenylboronic acid in the presence of the nanowires at room temperature (~23 °C). For example, addition of phenylboronic acid (**2**) to a mixture of iodobenzene (**1a**), sodium *t*-butoxide and Pd nanowires in water provided biphenyl product (**3a**) in an almost quantitative conversion after 24 hours (Table 1, entry 1). It is worth noting that the insoluble biphenyl product formed at water–air interface can be easily separated from the catalyst precipitated to the bottom of the solution (Fig. S4a and b of the ESI†). In contrast, the PVP-stabilized dispersed Pd nanoparticles (~5 nm) only afforded a relatively low yield of product (50%) for numerous attempts under these conditions (Table 1, entry 4). Indeed, early reports of the Suzuki reaction using dispersed Pd nanoparticles as the catalysts were typically carried out under reflux conditions (78 ~ 120 °C).[20–27] Our experimental results also revealed that the use of ethanol as a solvent generally shortens the time (~4 h) needed to complete the conversions (Table 1, entries 3, 5, 8, and 15). The enhanced reactivity can be largely attributed to improved solubility of the organic substrates in ethanol. Nonetheless, a binary combination of solvents in ethanol/water (2 : 3; v:v) offers comparably efficient conversions for a variety of substrates listed in Table 1 (entries 2, 9, 10, 12, 13, 16, 17, and 19). Importantly, the reaction between the phenyl chloride and phenylboronic acid can also proceed in high yields (entries 20 and 21) using polyethylene glycol as the solvent.

Table 1 Palladium nanowire-catalyzed Suzuki coupling of aryl halides and phenylboronic acids at room temperature[a]

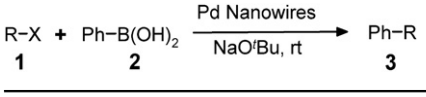

1 **2** **3**

Entry	R–X	Solvent	*t*/h	Product	% Conv.[b]
1	 **1a**	H_2O	24	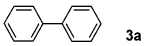 **3a**	99
2	**1a**	E/W[d]	4	**3a**	99
3	**1a**	EtOH	4	**3a**	99(93)[c]
4[e]	**1a**	H_2O	24	**3a**	50(40)[c]
5	 **1b**	EtOH	4	**3a**	95
6	**1b**	H_2O	24	**3a**	99
7	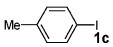 **1c**	H_2O	24	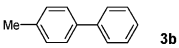 **3b**	44
8	**1c**	EtOH	4	**3b**	99
9	**1c**	E/W[d]	4	**3b**	99
10	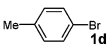 **1d**	E/W[d]	4	**3b**	99
11	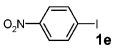 **1e**	H_2O	24	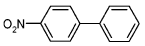 **3c**	76
12	**1e**	E/W[d]	4	**3c**	99
13	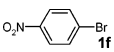 **1f**	E/W[d]	4	**3c**	99
14	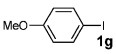 **1g**	H_2O	24	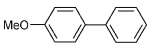 **3d**	72
15	**1g**	EtOH	4	**3d**	99
16	**1g**	E/W[d]	4	**3d**	99
17	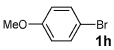 **1h**	E/W[d]	4	**3d**	99
18	 **1i**	H_2O	24	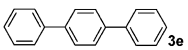 **3e**	27
19	**1i**	E/W[d]	4	**3e**	98
20[f]	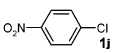 **1j**	PEG[g]	5	**3c**	91
21[h]	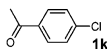 **1k**	PEG[g]	24	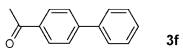 **3f**	87

[a] Reaction conditions: aryl halide (1 mmol), phenylboronic acid (1.2 mmol), NaO^{t}Bu (2 mmol), Pd nanowire catalyst (6.5 mol%), total solvent volume (10 mL). [b] GC-MS yields. [c] Values in parenthesis are isolated yields. [d] E/W refers to a solvent mixture of ethanol and water (2 : 3; v:v). [e] The entry relates to an analogous reaction using Pd nanoparticles as catalysts. [f] The reaction is carried out at 50 °C. [g] PEG refers to polyethylene glycol. [h] The reaction is carried out at 80 °C.

The catalytic activity of Pd nanowires are not limited to Suzuki reactions. It can be readily extended to other coupling reactions such as Heck reactions. Selected results for nanowire-catalyzed Heck reactions are summarized in Table S1 (ESI†). For instance, the chemical reaction of an iodobenzene with a styrene in the presence of the nanowire catalyst exhibits stereoselectivity with a high conversion (85%) for *trans*-coupling (Table S1, entry 1) at room temperature, albeit with the need of a polar aprotic solvent (dimethylformamide). Alternatively, the *trans*-coupling product can be favored in aqueous solvents at elevated temperatures (Table S1, entry 3), while its dispersed Pd nanoparticle counterpart gives rise to a low yield of product (Table S1, entry 4) under these conditions.

To benchmark the method, we further compared the activity of our Pd nanomaterials with bulk metal, dispersed nanoparticle

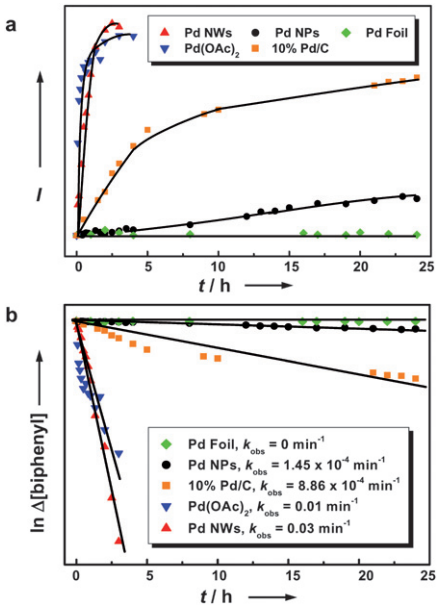

Fig. 2 (a) Formation of biphenyl product in ethanol as a function of time at room temperature by different catalysts including Pd nanowires, Pd nanoparticles, Pd foil, commercial Pd/C particles, and $Pd(OAc)_2$. The data points (average of two runs) were derived by acquiring the biphenyl absorption band (centered at 247 nm) for aliquot samples taken from the reaction at different time intervals. (b) Linear regression plot for the determination of the observed rate constants k_{obs}. The values were determined from a ln plot of the change in iodobenzene concentration *versus* time for respective reactions.

counterparts, and palladium(II) acetate [$Pd(OAc)_2$] as well as commercially available Pd catalyst (10% Pd/C) for coupling reactions by UV–vis spectroscopy. The formation of the biphenyl product for two different batch catalysts was monitored by quantitative absorption analysis of aliquot samples taken from the reaction at different time intervals as shown in Fig. 2a. The bulk metal (Pd foil, 1.6 mg), dispersed nanoparticles (~5 nm; 1 mg), 10% Pd/C catalyst (10 mg), and nanowires (1 mg) exhibit markedly different kinetic profiles for the coupling reaction between the phenylboronic acid and iodobenzene substrates at room temperature. The bulk metal did not show any catalytic activity toward the coupling reaction, while the nanoparticles and the Pd/C catalyst exhibited moderate catalytic activities. In contract, the Pd nanowires exhibit a rate constant that is about 200 and 34 times greater than that of the 5-nm nanoparticles and Pd/C catalyst, respectively (Fig. 2b). It is worth noting that the $Pd(OAc)_2$ catalyst shows a reactivity pattern similar to that of the Pd nanowires, but poses a substantial recycling challenge.

The scope of the Pd catalyst was further examined by recycling it from the reaction of iodobenzene with phenylboronic acid (Table 1, entry 1). It was observed that the catalyst exhibits consistent catalytic activity (~99%) over six recycles (Table S2 of the ESI†). It should be noted that the nanowire catalyst exhibits considerable thermal stability and mechanical robustness even after repeated ultrasonic treatment at elevated temperatures (Fig. S4c and d of the ESI†).

To provide insight into the nanocontact-induced catalytic activation, we performed first-principles density-functional theory (DFT) calculations on a contact between two Pd

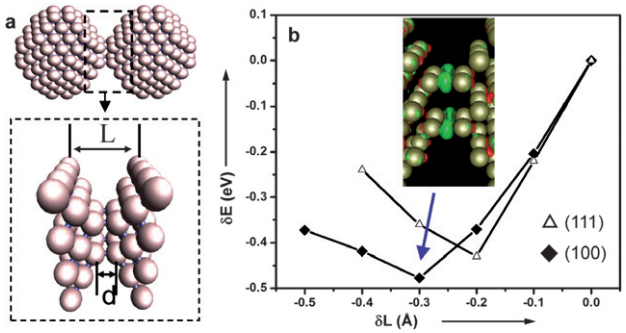

Fig. 3 (a) Geometry of two Pd nanoparticles contacted in the (100) direction. The enlarged contact region is indicated by an arrow. L is defined as the distance between two fixed outermost layers, and d is the bond length between two particles. (b) Total energy difference ($E - E_0$) for the (100) or (111) connection *versus* compression distance ($L - L_0$) of the two Pd particles. E_0 and L_0 are the total energy and the length of the contact as defined as the distance between two fixed outermost layers as shown in (a) (Inset: the isosurface of the excess electronic charge for the (100) connection in green).

nanoparticles of ~1.2 nm in diameter. The DFT calculations include the generalized gradient approximation,[28] using a plane wave basis (kinetic energy cutoff E_{cut} = 14.6 Ry) and pseudo-scalar relativistic soft pseudo-potentials.[29] Two Pd particles are contacted in either the (100) or (111) direction. The distance between two bulk layers, L, measures the length of the contact region. The bond length between two nanoparticles is denoted as d (see Fig. 3a). The electronic and atomic structures of the contact were calculated for different values of L. Two outermost layers of the contact region (see the enlarged contact region for 100 connection in Fig. 3a) are fixed in bulk structure during the structure optimization. This is consistent with a previous report that the change of L only has significant effects on a few atomic layers of the contact region.[30] The difference of the total energy ($\delta E = E - E_0$) upon compression of the contact ($\delta L = L - L_0$, L_0 = 8.25 Å for 100 connection and 11.76 Å for 111 connection, respectively) is shown in Fig. 3b, where E_0 is the total energy of the two nanoparticles and L_0 is the length of the contact prior to compression. For the lowest energy state, L and d are found to be 7.95 (11.56) Å and 2.66 (2.60) Å for 100 (111) connection, respectively. The charge redistribution in the contact region due to the bonding of two particles of 100 connection is shown in the inset of Fig. 3b, where the green color represents the accumulation of electrons, and the red color is the depletion of electrons. Clearly, electron transfer (*ca.* 1.2 e) occurs from the nanoparticles to the interfacial region to form bonds. For the (100) connection, the amount of the charge transfer is about 1.2 electrons, while for the (111) connection, it is about 1.1 electrons. This charge redistribution makes the nanocontact highly attractive to organic molecules, thus resulting in the enhanced catalytic reactivity of the nanomaterials.

In conclusion, we have reported the synthesis of novel Pd nanostructures *via* a combination of the PVP-templated method and a slow particle crystallization process. The as-prepared nanostructured materials show distinctive catalytic properties in sharp contrast to bulk metal and individual nanoparticles. These studies are important not only because they provide a potential platform to study the underlying principle that governs the catalytic reactivity of nanomaterials, but also because they shed insight into designing highly reactive and recyclable catalytic systems for organic transformations. Along these lines, we are currently investigating electron transport within the polycrystalline nanowires and exploring the fabrication of polycrystalline nanomaterials with various material compositions.

Acknowledgements

This work was supported by the NUS Academic Research Fund (R-143-000-317 and R-143-000-342) and a Young Investigator Award (R-143-000-318) to X. L. by the NUS. X. L. is grateful for H. C. Zeng for helpful discussions. We thank B. Liu, C. Tang, and Y. Nie for technical assistance. C. Z. acknowledges the NUS Start-up Fund (R-144-000-237). Computations were performed at the Centre for Computational Science and Engineering at NUS.

References

1 J. Grunes, J. Zhu and G. A. Somorjai, *Chem. Commun.*, 2003, 2257.
2 G. A. Somorjai and R. M. Rioux, *Catal. Today*, 2005, **100**, 201.
3 Z. Duan, S. Ranjit, P. Zhang and X. Liu, *Chem.–Eur. J.*, 2009, **15**, 3666.
4 D. Astruc, F. Lu and J. R. Aranzaes, *Angew. Chem., Int. Ed.*, 2005, **44**, 7852.
5 N. Tian, Y. Zhou, S. Sun, Y. Ding and Z. L. Wang, *Science*, 2007, **316**, 732.
6 H. Song, R. M. Rioux, J. D. Hoefelmeyer, R. Komor, K. Niesz, M. Grass, P. Yang and G. A. Somorjai, *J. Am. Chem. Soc.*, 2006, **128**, 3027.
7 X. Liu, N. Wu, B. H. Wunsch, R. J. Barsotti Jr. and F. Stellacci, *Small*, 2006, **2**, 1046.
8 X. Lu, H.-Y. Tuan, J. Chen, Z.-Y. Li, B. A. Korgel and Y. Xia, *J. Am. Chem. Soc.*, 2007, **129**, 1733.
9 X. Liu, *Angew. Chem., Int. Ed.*, 2009, **48**, 3018.
10 C. Jiang, F. Wang, N. Wu and X. Liu, *Adv. Mater.*, 2008, **20**, 4826.
11 J. Yuan, X. Liu, O. Akbulut, J. Hu, S. L. Suib, J. Kong and F. Stellacci, *Nat. Nanotechnol.*, 2008, **3**, 332.
12 U. Landman, R. N. Barnett, A. G. Scherbakov and P. Avouris, *Phys. Rev. Lett.*, 2000, **85**, 1958.
13 E. Tosatti, S. Prestipino, S. Kostlmeier, A. Dal Corso and F. Di Tolla, *Science*, 2001, **291**, 288.
14 D. O. Demchenko and L.-W. Wang, *Nano Lett.*, 2007, **7**, 3219.
15 B. Pérez-García, J. Zúñiga-Pérez, V. Muñoz-Sanjosé, J. Colchero and E. Palacios-Lidón, *Nano Lett.*, 2007, **7**, 1505.
16 Y. Sun and Y. Xia, *Science*, 2002, **298**, 2176.
17 Y. Sun, B. Gates, B. Mayers and Y. Xia, *Nano Lett.*, 2002, **2**, 165.
18 Y. Xiong, J. Chen, B. Wiley and Y. Xia, *J. Am. Chem. Soc.*, 2005, **127**, 7332.
19 Y. Xia, P. Yang, Y. Sun, Y. Wu, B. Mayers, B. Gates, Y. Yin, F. Kim and H. Yan, *Adv. Mater.*, 2003, **15**, 353.
20 L. K. Yeung and R. M. Crooks, *Nano Lett.*, 2001, **1**, 14.
21 M. Ooe, M. Murata, T. Mizugaki, K. Ebitani and K. Kaneda, *J. Am. Chem. Soc.*, 2004, **126**, 1604.
22 E. H. Rahim, F. S. Kamounah, J. Frederiksen and J. B. Christensen, *Nano Lett.*, 2001, **1**, 499.
23 J. C. Garcia-Martinez, R. Lezutekong and R. M. Crooks, *J. Am. Chem. Soc.*, 2005, **127**, 5097.
24 R. M. Crooks, M. Zhao, L. Sun, V. Chechik and L. K. Yeung, *Acc. Chem. Res.*, 2001, **34**, 181.
25 L. Strimbu, J. Liu and A. E. Kaifer, *Langmuir*, 2003, **19**, 483.
26 S.-W. Kim, M. Kim, W. Y. Lee and T. Hyeon, *J. Am. Chem. Soc.*, 2002, **124**, 7642.
27 R. Narayanan and M. A. El-Sayed, *J. Phys. Chem. B*, 2004, **108**, 8572.
28 J. P. Perdew, K. Burke and M. Ernzerhof, *Phys. Rev. Lett.*, 1996, **77**, 3865.
29 N. Troullier and J. L. Martins, *Phys. Rev. B: Condens. Matter Mater. Phys.*, 1991, **43**, 1993.
30 C. Zhang, R. N. Barnett and U. Landman, *Phys. Rev. Lett.*, 2008, **100**, 046801.

